Experiments with Nonneutral Plasmas

T. M. O'Neil

University of California San Diego, Physics Department 0319, La Jolla, CA92129-0319

Abstract. Selected experiments with nonneutral plasmas are discussed. These include the laser cooling of a pure ion plasma to a crystalline state, a measurement of the Salpeter enhancement factor for fusion in a strongly correlated plasma and the measurement of thermally excited plasma waves. Also, discussed are experiments that demonstrate Landau damping, trapping and plasma wave echoes in the 2D ***ExB*** drift flow of a pure electron plasma, which is isomorphic to the 2D ideal flow (incompressible and inviscid flow) of a neutral fluid.

INTRODUCTION

When I became Norman's first graduate student in the early days of UCSD, he was just finishing his beautiful body of work on correlations, fluctuations and collisions in weakly correlated, thermal equilibrium plasmas [1, 2, 3, 4], and the first problem that he asked me to work on was a calculation of the triple correlation function [5]. Today, I will discuss recent experiments with nonneutral plasmas (pure ion and pure electron plasmas), selecting examples that illustrate correlation and fluctuation physics. At the end of my talk, I will discuss an example that illustrates my thesis research [6] with Norman on the nonlinear saturation of Landau damping through the trapping of particles in wave troughs, but in a novel context. Landau damping and trapping are not limited to plasma waves that are excited in Vlasov plasmas, but also can occur when Kelvin waves are excited on a vortex in an ideal fluid, that is, an incompressible and inviscid fluid [7]. As we will see, a Kelvin wave analogue of plasma wave echoes also exists in such fluids [8]. The 2 D dynamics of an ideal fluid is well modeled by the 2D ***ExB*** drift dynamics of pure electron plasma.

Figure 1 illustrates the confinement of pure ion plasma in a Malmberg-Penning trap [9, 10]. A conducting cylinder is divided axially into three sections, with the central section grounded and the two end sections held at a positive potential. The plasma resides in the region of the central cylinder, with axial confinement provided by electric fields and radial confinement provided by a uniform axial magnetic field. Because the ion plasma is not neutralized, Gauss's law requires that there be a radial electric field, and the radial electric field and axial magnetic field together cause the plasma to undergo ***ExB*** drift rotation.

The Physics of Plasma-Driven Accelerators and Accelerator-Driven Fusion
AIP Conf. Proc. 1721, 020002-1–020002-14; doi: 10.1063/1.4944011

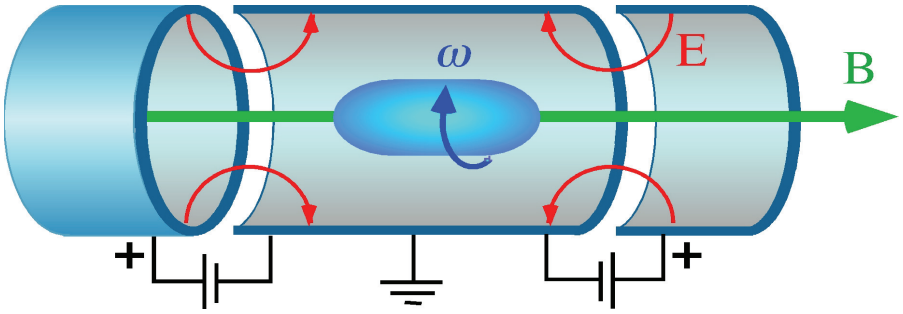

FIGURE 1. Schematic diagram of Malmberg-Penning trap for a pure ion plasma

An important property distinguishing these plasmas from neutral plasmas is that these plasmas can come to a state of thermal equilibrium while they are confined [11, 12]. As is well known, a neutral plasma cannot be confined by static electric and magnetic fields and also be in a state of thermal equilibrium [12]. When a neutral plasma is confined by such fields, there is always free energy, and the free energy tends to drive instabilities. That is why the confinement of neutral plasmas is notoriously difficult. In contrast, a plasma with a single sign of charge that is confined in a state of thermal equilibrium has no free energy and is guaranteed to be stable and quiescent.

For a cylindrically symmetric trap, both the total Hamiltonian and the total canonical angular momentum for the ions are constants of the motion, so the Boltzmann distribution takes the form [12]

$$f = C\exp[-(h-\omega p_\theta)/kT]\ , \tag{1}$$

where C is a constant, k is the Boltzmann constant, T is the plasma temperature, and ω is the plasma rotation frequency. The quantity $h = mv^2/2 + e\varphi(r,z)$ is the 1-particle Hamiltonian, where v is the particle velocity, and $e\varphi(r,z)$ is the potential energy. The quantity $p_\theta = mv_\theta r + eBr^2/2c$ is the 1-particle canonical angular momentum, where the first term is the usual mechanical contribution and the second term is the vector potential contribution. Here, (r,θ,z) is a cylindrical coordinate system with the z-axis coincident with the axis of the trap. The combination

$$h_{rot} = h - \omega p_\theta = m(\mathbf{v} - \omega r\hat{\theta})^2/2 + e\varphi(r,z) + m\omega(\Omega_c - \omega)r^2/2 \tag{2}$$

is the 1-particle Hamiltonian in a frame rotating with frequency ω. Here, $\Omega_c = eB/mc$ is the ion cyclotron frequency. From the first term in Eq. (2), one can see that the velocity dependence of the Boltzmann distribution is a Maxwellian in the rotating frame. The spatial dependence for the distribution is determined by the last two terms in Eq. (2), which together are the potential energy of an ion in the rotating frame. The last term is the correction to the potential energy due to rotation and consists of the centrifugal potential energy, $-m\omega^2 r^2/2$, plus the potential energy associated with the inward radial electric field that is induced by rotating through the magnetic field, that is, the quantity

$$-\int_0^r eE_r\,dr = \int_0^r e(\omega rB/c)dr = m\Omega_c\omega r^2/2 \tag{3}$$

.

To see that the Boltzmann distribution corresponds to a confined plasma, let us start at the center of the trap (i.e., $r=z=0$) and first move toward larger values of z. As z approaches the positively biased end cylinders, the second term in Eq. (2) becomes large and positive, forcing the distribution to become exponentially small. If one moves radially outward from the center and if $\Omega_c > \omega$, the third term becomes

large, again forcing the distribution to become exponentially small. The effective potential in the rotating frame is a potential well, and the plasma simply comes to thermal equilibrium in that well.

Another way to understand the thermal equilibrium state starts with the observation that the third term in Eq. (2), that is, the term that provide the correction due to rotation, is quadratic in r [12]. Suppose that the ion plasma were not confined by rotation through the magnetic field, but rather by an imaginary cylinder of uniform negative charge. Gauss's law implies that the cylinder would produce an inward radial electric field proportional to *r*, or equivalently, a radial potential that is a quadratic potential in *r*. By choosing the negative charge density to have a value determined by the relation $\omega_p^2 = \omega(\Omega_c - \omega)$, where $\omega_p^2 = 4\pi ne^2/m$ is the square of the plasma frequency and n is the density, the potential energy of an ion in the imaginary cylinder of uniform negative charge would be identical to the potential energy due to the third term in Eq. (2).

This is a useful way to think about the ion potential energy, since we know what will happen if we throw a bunch of ions into a potential well produced by the cylinder of uniform negative charge and the positively biased end cylinders. The ions will match their density to the density of the uniform negative charge filling the well up to some surface of revolution where the supply of ions is exhausted, and there the density will fall off on the scale of a Debye length. That is, for small Debye length, the plasma density is uniform out to the surface of revolution and there drops abruptly to zero. The temperature and rotation frequency also are uniform inside the thermal equilibrium plasma; if they were not, viscosity and heat conduction would produce entropy, and that is not possible for a state of maximum entropy.

Figure 2 shows a schematic diagram of a Malmberg-Penning trap that is used to confine Mg^+ ion plasmas at UCSD [13]. Provision is made for a laser beam directed along the magnetic field and for a laser beam transverse to the field. The beams are used to laser cool the plasma and to diagnose the plasma by measurement of the laser induced fluorescence at axial position *z*=0.

The thermal equilibrium state is predicated on the assumption of a cylindrically symmetric trap, and although care is taken to insure a high degree of cylindrical symmetry in the trap and fields, there inevitably remain small construction errors and field errors that break the cylindrical symmetry and exert a weak drag torque on the rotating plasma. This weak torque changes the total canonical angular momentum and produces a slow outward radial drift that leads to plasma loss over relatively long times, say, of order an hour. Of course, the ions of the rotating plasma are in thermal equilibrium with each other, but not with the stationary wall. To counteract the torque from the stationary field asymmetries and achieve arbitrarily long confinement, a field asymmetry that rotates slightly faster than the plasma is applied using the azimuthally sectored section of the wall labeled "rotating wall". The name derives from the notion that the rotating field asymmetry tricks the plasma into thinking that the wall is rotating.

In recent years, Norman and his collaborators have pursued such a rotating field scheme as a means of driving current in an FRC [14].

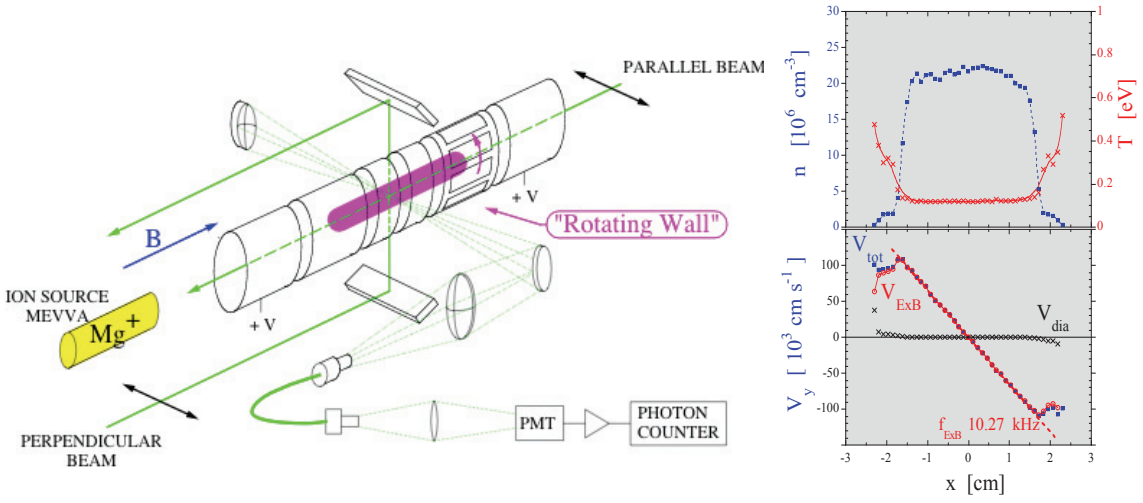

FIGURE 2. Schematic diagram of a Malmberg-Penning trap used to confine Mg^+ ions at UCSD.

The inset in Fig. 2 shows a plot of the density n, temperature T and azimuthal velocity V as a function of radius for an 18-hour-old plasma [13]. To see that the plasma is very near to thermal equilibrium, note that the density and temperature are essentially constant inside the plasma and that the mean azimuthal velocity is nearly a linear function of radius, implying near uniform rotation. The full velocity distribution is nearly Maxwellian in the rotating frame of the plasma. The macroscopic state of the thermal equilibrium plasma is well described by the Boltzmann distribution.

CORRELATION AND CRYSTALS

To understand the microscopic order, the Gibbs distribution is needed. This distribution is of the same form as the Boltzmann distribution, except that the 1-particle Hamiltonian h_{rot} is replaced by the N-particle Hamiltonian H_{rot}, including the ion-ion interactions. Using the same argument as used for the Boltzmann distribution, one can show that the Gibbs distribution for the magnetically confined ion plasma differs only by rotation from the Gibbs distribution for an ion plasma confined by a cylinder of uniform neutralizing negative charge [12]. All of the correlation properties are the same for the two systems.

A single species of point charges imbedded in a uniform neutralizing background charge is called a One Component Plasma (OCP) and has been a favorite theoretical model for the study of correlation effects [15]. All of the theory developed for correlations in a thermal equilibrium OCP can be taken over and applied to the magnetically confined pure ion plasma; indeed, the magnetically confined plasma is a simple laboratory model of an OCP.

For an OCP large enough that the bulk free energy dominates over surface free energy, the state of correlation is determined solely by the coupling parameter $\Gamma = e^2 / akT$, where $a = \sqrt[3]{3/4\pi n}$ is the Wigner-Seitz radius, essentially the inter-particle spacing [12]. For $\Gamma << 1$ theory predicts that the OCP is weakly correlated, for $\Gamma \sim 2$ stronger correlation and OCP begins to exhibit the local order characteristic of a liquid, and for $\Gamma = 178$ that there is a phase transition to a body-centered-cubic (bcc) crystal.

Figure 3. shows an experimental image of a Be^+ ion plasma that has been laser cooled to the bcc crystal state by John Bollinger and collaborators of the NIST ion storage group [16]. The plasma is a small spheroid with dimensions of order a millimeter, density of $n \simeq 4 \times 10^8 cm^{-3}$ and temperature $T < 10mK$, which corresponds to a coupling parameter $\Gamma > 200$. This value is well into the crystal regime. From the schematic diagram in the center of the figure, one can see that the NIST group orients the Malmberg-Penning trap vertically, rather than horizontally as was shown in Figs. 1 and 2. There is an axial laser cooling beam and a transverse laser cooling beam. In the image from the side view camera, one sees scattered light from both the axial and the transverse laser beams, with the latter being more intense. The strobed top view camera shows light largely from the transverse laser beam, and one can see that the ions are arranged in a crystal structure. A blow up of a small region shows the (100) plane of a bcc crystal with lattice spacing in close agreement with the theory prediction, based on the magnetic field strength and the rotation frequency. Interestingly, the light seen here is scattered by individual atoms, collected in synchronously strobed time windows over many rotations of the crystal structure.

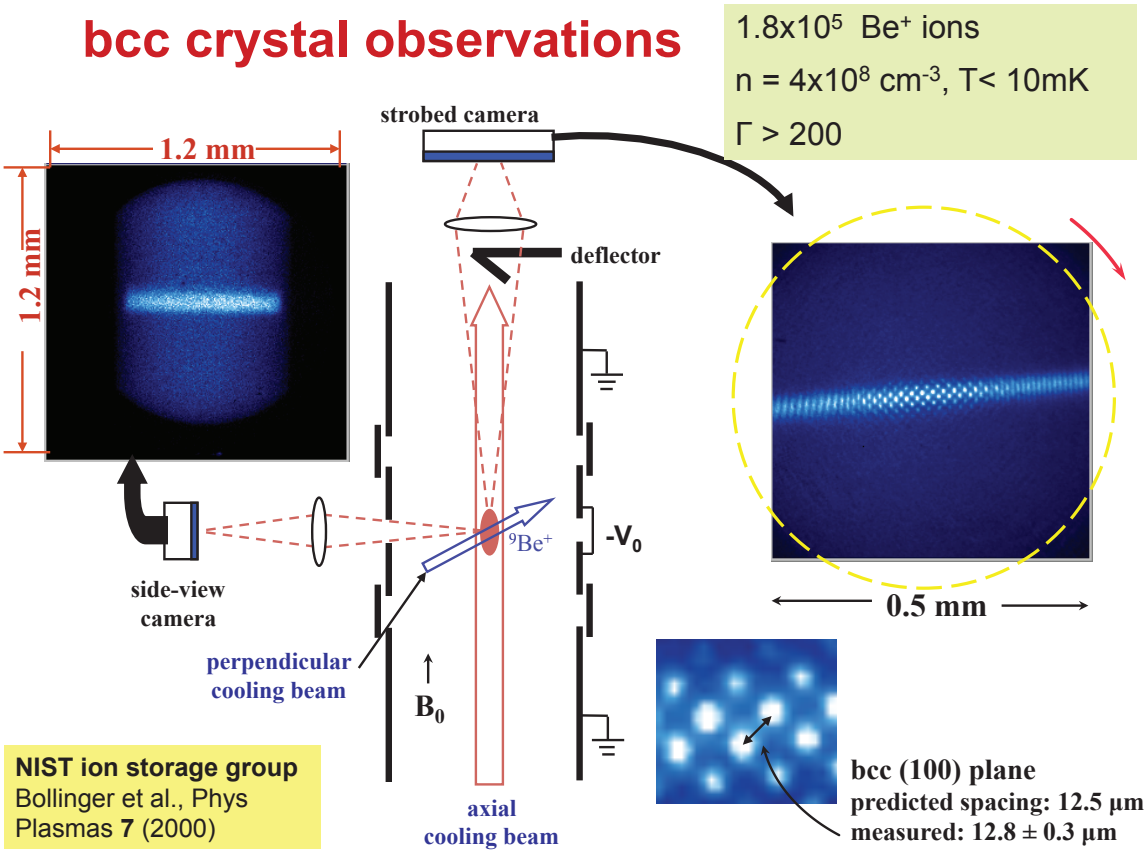

FIGURE 3. Schematic diagram of a Malmberg-Penning trap used by the NIST ion storage group to cool a Be^+ ion plasma to a bcc crystal state.

CORRELATION ENHANCEMENT OF CLOSE COLLISIONS

Norman often thought about correlation effects in terms of dressed test particles, where each particle is dressed in a Debye cloud [2,17]. Thinking along similar lines, Ed Salpeter predicted that Debye shielding, and more generally correlations, enhance the thermonuclear fusion rate, for example in stars [18]. The shielding reduces the Coulomb repulsion between two colliding ions, allowing the ions to approach one another more closely and increasing the probability of tunneling through to produce a fusion reaction. The enhancement of the fusion rate is approximately of the form $R_{enhanced} = R_0 e^{\Gamma}$, where $R_{enhanced}$ is the enhanced rate and R_0 is the rate neglecting shielding and correlation. The exponential enhancement factor assumes that Γ is not too large, and that restriction is satisfied for the experiments discussed here.

We want to measure this enhancement factor using the Mg^+ plasma described in Fig. (2). Since there aren't any fusion reactions in such a cryogenic ion plasma, we need a stand in for fusion reactions. When a plasma is strongly magnetized and has very low temperature, the cyclotron radius $r_c = \sqrt{kT/m}/\Omega_c$ can be smaller than the classical distance of closest approach $b = e^2/kT$. Then the cyclotron action is an adiabatic invariant that is nearly conserved in collisions [19]. The modifier "nearly" is used here since an adiabatic invariant is not an exact constant of the motion, but rather is changed by an exponentially small amount. Of course, close energetic collisions are most effective in changing the adiabatic invariant and liberating cyclotron energy. This sounds a lot like nuclear fusion, where it is the close energetic collisions that are

most effective in liberating the nuclear energy. In fact, Dan Dubin has shown that the analogy is quantitatively correct [20].

A measure of the rate of liberation of cyclotron energy is the collisional equipartition rate $\nu_{\perp\|}$, where $dT_\| / dt = \nu_{\perp\|}(T_\perp - T_\|)$. Here, $T_\|$ is the temperature associated with velocity components parallel to the magnetic field and $T_\perp$ is the temperature associated with velocity components perpendicular to the field. Dubin's enhanced equipartition rate [20] is given by $(\nu_{\perp\|})_{enhanced} = (\nu_{\perp\|})_0 e^\Gamma$, which is the same enhancement as that for the fusion rate. For the case of fusion, the exponentially small tunneling factor is averaged over a thermal distribution of collisions, and for the case of equipartition the exponentially small factor for breaking the adiabatic invariant is averaged over a thermal distribution of collisions.

Figure (4) shows measurements of the equipartition rate versus temperature for two values of the density [21]. The abscissa on the bottom is a logarithmic scale of temperature in electron volts, and the abscissa on the top is the corresponding ratio of r_c/b for the magnetic field strength 3 Tesla. The ordinate is a logarithmic scale of the equipartition rate.

For the lower density, $n = 1.2 \times 10^6 cm^{-3}$, the solid blue curve is the predicted equipartition rate neglecting the enhancement, and the dashed blue curve is the predicted rate including the enhancement. The points are the measurements. One can see that the rate follows the usual scaling $1/T^{3/2}$ for large T and falls of dramatically for sufficiently small T (i.e., $r_c/b < 1$), confirming the effect of the adiabatic invariant. For this value of density, the blue diagonal line in the lower left hand corner of the figure shows the value of Γ versus temperature. Since Γ is smaller than unity over the full range of measurements, the predicted enhancement is small, the solid and dashed blue curves are very close to each other, and the measurement points do not distinguish between the two curves.

The red curves and points are for the higher density, $n = 2 \times 10^7 cm^{-3}$, and for this density one sees that Γ values as large as 10 are accessed in the measurements. The points now favor the dashed curve, providing evidence of enhancement.

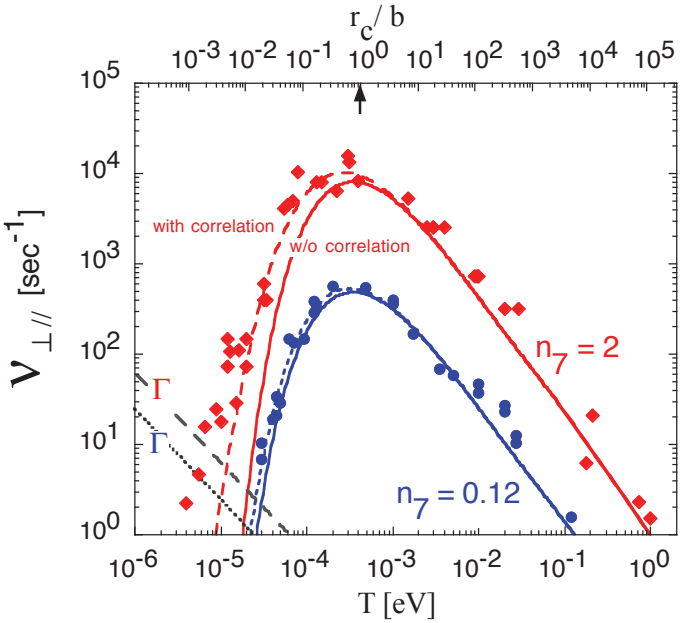

FIGURE 4. Predicted and measured equipartition rates versus temperature.

Figure (5) shows a log-log plot of the enhancement factor versus Γ. Again the points are measurements and the curves are e^Γ and three other more accurate predictions for the enhancement factor [22]. On this log-log plot, the curves are nearly indistinguishable. One sees a nine orders of magnitude enhancement of close energetic collisions.

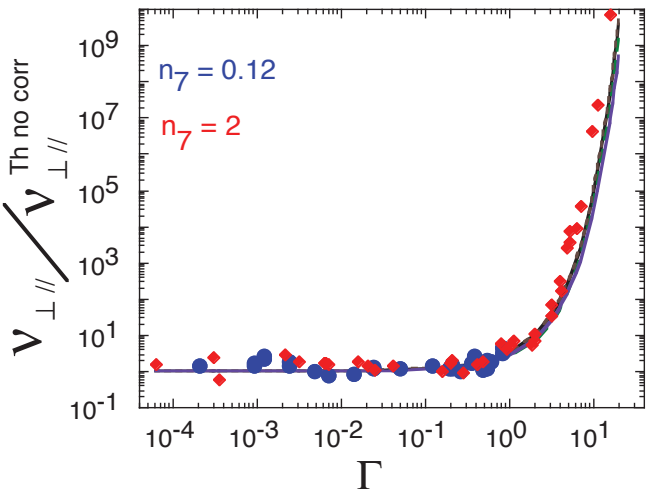

FIGURE 5. The measured enhancement factor versus Γ, compared to theoretical predictions for the enhancement factor.

THERMAL FLUCTUATIONS

Recent experiments have measured thermal level fluctuations of plasma modes, or more precisely Trivelpiece-Gould modes, in pure electron plasmas [23]. Figure 6 shows the result of a transmission experiment in which a sinusoidal voltage is applied to a driver electrode, and the response is measured on a well-separated receiver electrode. The driver frequency is swept, and when the frequency matches the frequency of a standing mode, the mode is excited and detected on the receiver electrode. The standing modes differ in the number of half wavelengths that fit in the length of the plasma column (i.e., $\lambda = L_p / 2m_z$). Figure 6 shows the received signal for three drive amplitudes, including zero amplitude. For zero drive amplitude, that is, thermal excitation, the modes m_z=1,3,4,5 are still received. The coupling to the m_z=2 mode is suppressed with this electrode geometry, and the resonance labeled RW is the signal from the "rotating wall" drive.

Figure 7 shows the received spectra of the thermally excited m_z=1 mode for four different plasma temperatures. The mode frequency increases with temperature according to the Bohm-Gross correction to the dispersion relation, so the four curves are displaced in frequency relative to one another. The width of each spectral peak is determined by the total damping rate for the mode, which is the sum of the intrinsic mode damping and the load damping, that is, the damping due to resistance in the measuring circuit. The intrinsic mode damping includes Landau damping, which becomes large as the temperature increases, substantially increasing the width of the resonance.

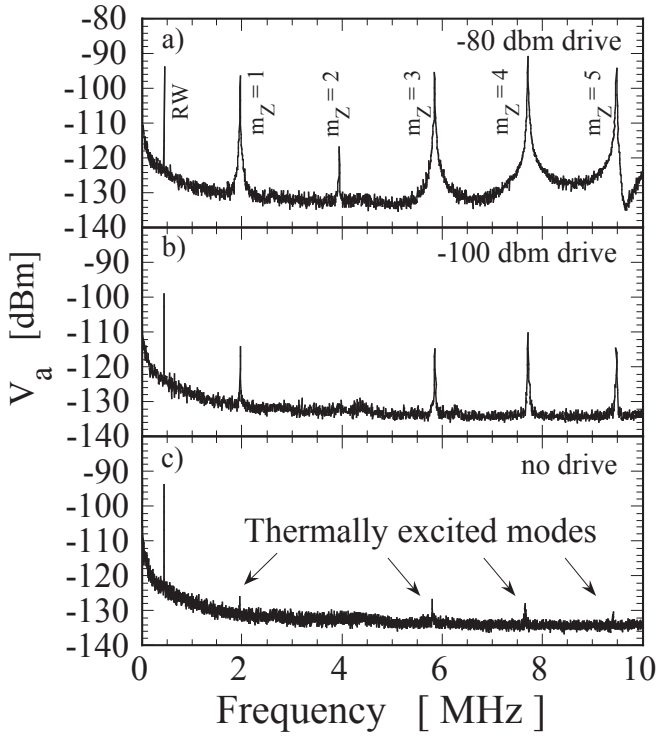

FIGURE 6. Spectrum of $m\theta$=0, m_z=1,2,…,5 Trivelpiece-Gould modes excited at three levels of drive amplitude, including zero drive, that is, thermally excitation.

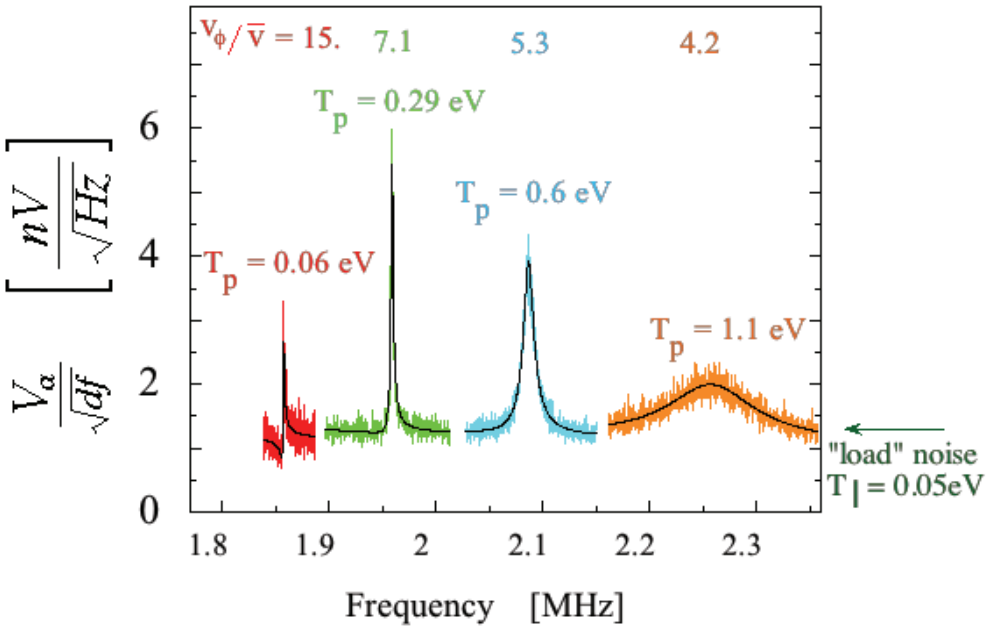

FIGURE 7. Thermal spectrum of the m_z=1 mode for 4 different plasma temperatures.

Norman's theoretical calculations of fluctuations in thermal equilibrium plasmas are not directly applicable to these experiments, because here the mode is coupled to a measuring circuit, characterized by

an impedance. The circuit resistance both damps the mode and excites the mode through thermal noise in the resistor.

Figure 8-a shows a schematic diagram of the plasma and measuring circuit (load), and Fig. 8-b shows an equivalent circuit, with the plasma impedance and load impedance in parallel between ground and the receiver electrode. From the equivalent circuit diagram, one obtains the generalized Nyquist formula

$$\frac{V_a^2(f)}{df} = 4kT_p Z_m^{\mathrm{Re}} \left| \frac{Z_l}{Z_m + Z_l} \right|^2 + 4kT_l Z_l^{\mathrm{Re}} \left| \frac{Z_m}{Z_m + Z_l} \right|^2 , \qquad (4)$$

where T_p is the plasma temperature and T_l is the load temperature. The quantity Z_m is the impedance of the plasma near the resonance of mode m, and Z_l is the load impedance. In Eq. (4) the sum of the squared voltages are added, since the shot noise in the plasma is uncorrelated with the noise in the load resistor. The first term in Eq. (4) is a Lorentzian resonance spectrum characterizing the mode, with slight shifts in the frequency and width due to interaction of the mode with the load. When the plasma temperature is much higher than the load temperature, the Lorentzian dominates the observed spectrum, as shown in Fig. 7 for the higher temperature measurements. At the lower temperature measurements (e.g.,kT_p=0.06 eV) the Lorentzian is distorted by the influence of the second term. Nevertheless, using the known impedance for the load and the shape of the measured spectrum, the plasma temperature T_p can be extracted. The black curves in Fig. 7 are the best fits to Eq. (4), determining T_p.

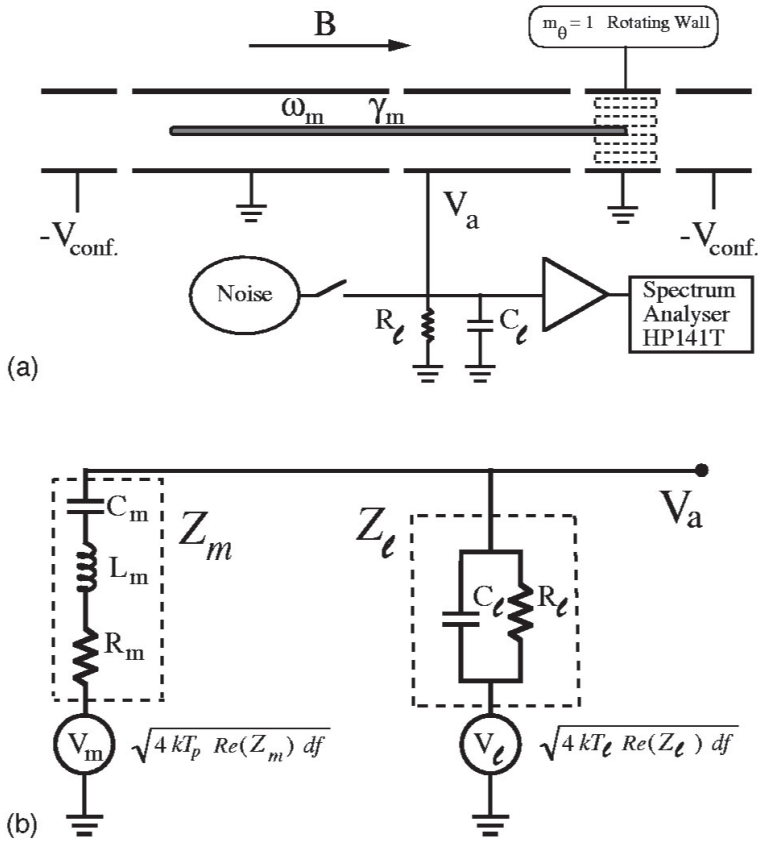

FIGURE 8. (a) Schematic diagram of Malmberg-Penning trap and measuring circuit. (b) Equivalent circuit for plasma mode and receiver

Figure 9 shows a comparison of the plasma temperature measured from the fluctuation spectra with the plasma temperature measured by dumping the plasma out axially along the field lines to a velocity analyzer. Of course, this latter measurement destroys the plasma. Since the agreement between the two

temperature measurements is good, the fluctuation measurements can be used as a non-destructive temperature measurement [23].

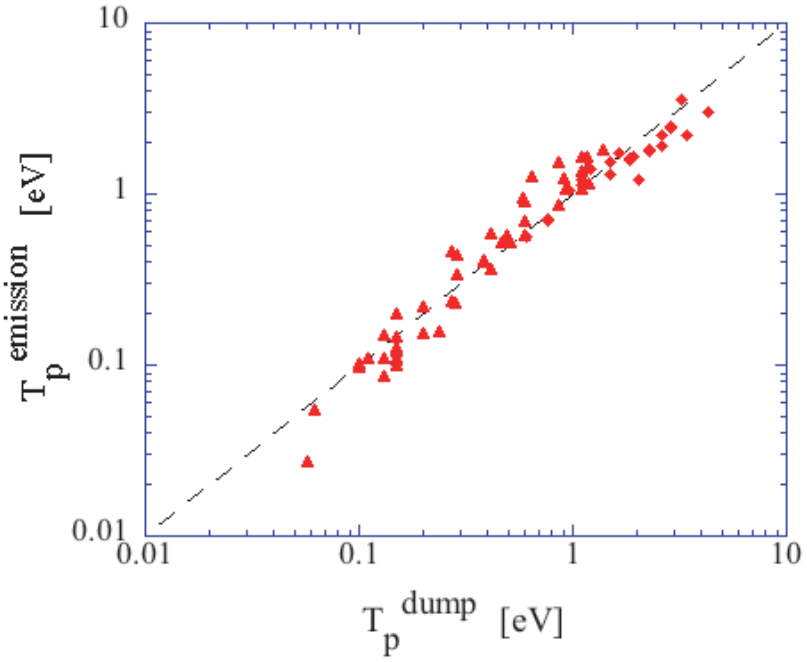

FIGURE 9. Comparison of plasma temperature measured from the thermal fluctuations with plasma temperature measured by dumping plasma to a velocity analyzer.

LANDAU DAMPING, TRAPPING, AND ECHOES IN IDEAL FLUIDS

Figure 10 shows a schematic diagram of a pure electron plasma experiment that can be used to model the ideal (incompressible and inviscid) flow of a neutral fluid [7]. The apparatus is operated in an inject-hold-dump sequence. Electrons from a hot filament are trapped and held long enough for interesting ***ExB*** drift flows to take place. The cylinder at the far end is then switched to ground, dumping the electrons out along the magnetic field lines to a phosphor screen, which is imaged by a CCD camera. In this way, the number of electrons along each field line is imaged.

In the experiments, frequencies are ordered as $\Omega_c >> \omega_B >> \omega_D$, where Ω_c is the cyclotron frequency, $\omega_B \approx \pi\overline{v} / L_p$ is the axial bounce frequency and ω_D is the frequency characterizing the ***ExB*** drift motion. With this ordering the cross-magnetic-field electron dynamics can be described as 2-D, bounce-averaged ***ExB*** drift dynamics. The density $n(r,\theta,t)$ evolves according to the coupled 2-D continuity equation and Poisson's equation, which are identical to Euler's equations for the flow of an ideal fluid [7]. In this equivalence, the electric potential corresponds to the stream function, the ***ExB*** drift velocity to the fluid velocity, and the electron density to the vorticity.

One advantage of the electron system is that the vorticity is imaged directly; one need not take the curl of measured flow velocities, which can include noise. Also, the effective viscosity is very low, allowing large Reynolds number ($R>10^5$), and the boundary condition at the wall is free-slip, so there are no boundary layers at the wall. Good shot to shot reproducibility enables movies of vorticity evolution, with subsequent frames in the movie imaged at successively later dump times. The system has been used for a wide variety of studies involving vortex dynamics and 2-D turbulence [24].

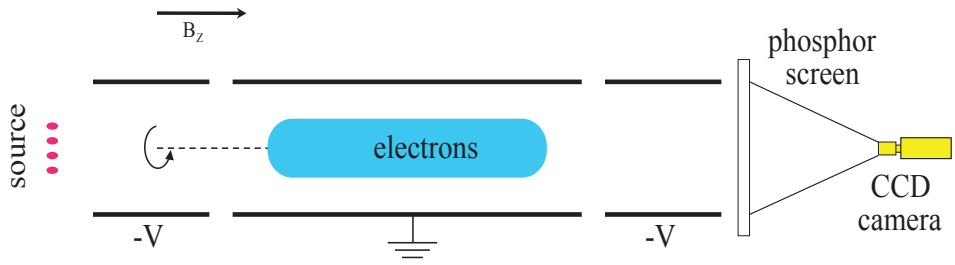

FIGURE 10. Schematic diagram of pure electron plasma experiment that is used to model the flow of an ideal fluid.

Figure 11 shows an experimental demonstration of the fluid equivalent of Landau damping and nonlinear saturation through trapping [7]. My thesis research with Norman, was a theoretical study of such saturation for the Landau damping of a plasma wave in a Vlasov plasma [5]. Of course, the Vlasov flow occurs in the phase space (x, v_x) and the ***ExB*** drift flow (and isomorphic ideal fluid flow) occur in (r,θ) space, but both flows are 2 D incompressible flows and nearly identical near the critical layer of the Landau resonance.

In the language of fluid dynamics, Fig. 11 (a) shows images of a vortex at three subsequent times. An m=2 Kelvin wave has been excited on this vortex; one can see a quadrupole distortion of the vortex in the T=0 image and cat's eye orbits at the resonant layer in the later images. The critical layer occurs at the radius where the Kelvin wave phase velocity matches the rotational flow velocity of the fluid in the vortex, and the resonant interaction between the wave and the fluid elements there gives rise to Landau damping of the wave. Figure 11 (b) shows the quadrupole moment of the vortex, effectively the amplitude of the m=2 wave, versus time. One sees an initial decay due to Landau damping followed by nonlinear saturation due to trapping.

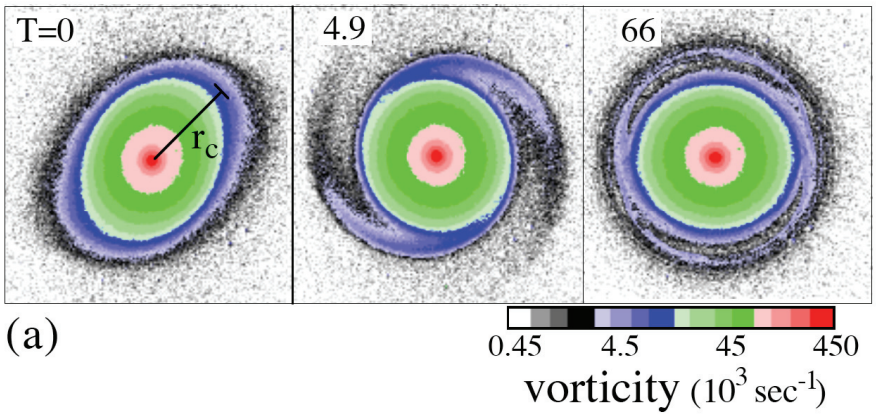

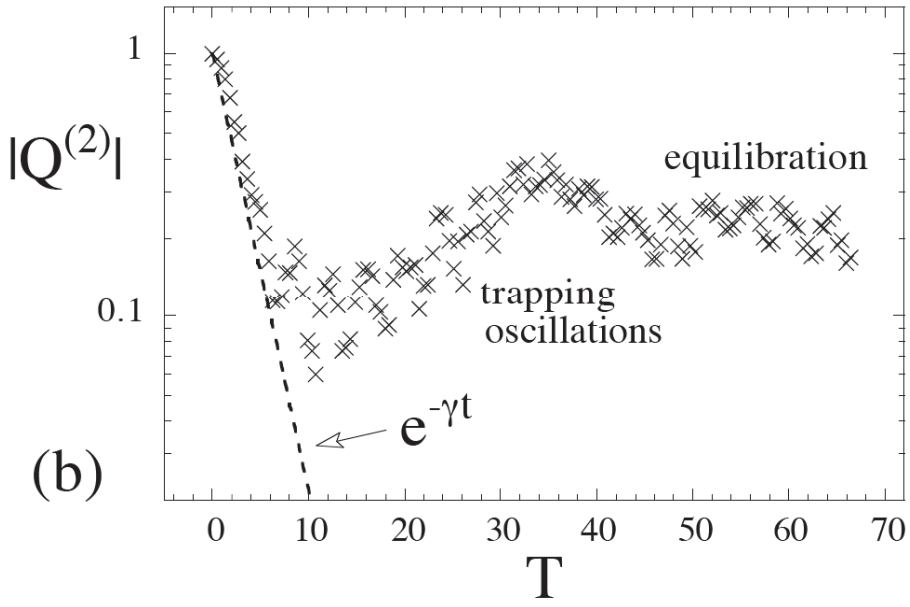

FIGURE 11. Experimental demonstration of the fluid equivalent of Landau damping and nonlinear saturation through trapping oscillations.

Figure 12 shows results from an experiment that demonstrates the existence of a fluid echo [8], a direct analogue of the plasma wave echo [25]. In this figure, the images (a) --- (f) are difference measurements, where the image of the unperturbed density is subtracted electronically from the image of the perturbed density, leaving only the perturbation. In image (a), one sees that an m=2 mode has been excited. Below the figures is a plot of the wave signal measured on a wall electrode, and one sees that the signal damps away as the m=2 perturbation phase mixes. One can think of Landau damping as resulting from such phase mixing. By the time of image (c), the perturbation is thoroughly phase mixed and the wall signal is nearly zero. Just before image (d), an m=4 mode is excited, rippling up the unperturbed density to form an l=4 density perturbation. This perturbation then phase mixes and the corresponding wall signal damps away. However, the m=4 field also ripples up the phase mixed ripple left over from the original m=2 mode, and a portion of this nonlinear m=2 ripple begins to un-phase mix causing an echo at the time of image (f). Of course, this reversal of phase mixing can be degraded by "non-ideal" flow effects. In these electron plasmas, the maximum coherence time for echoes is limited by extraneous rotational drifts associated with the end fields [8].

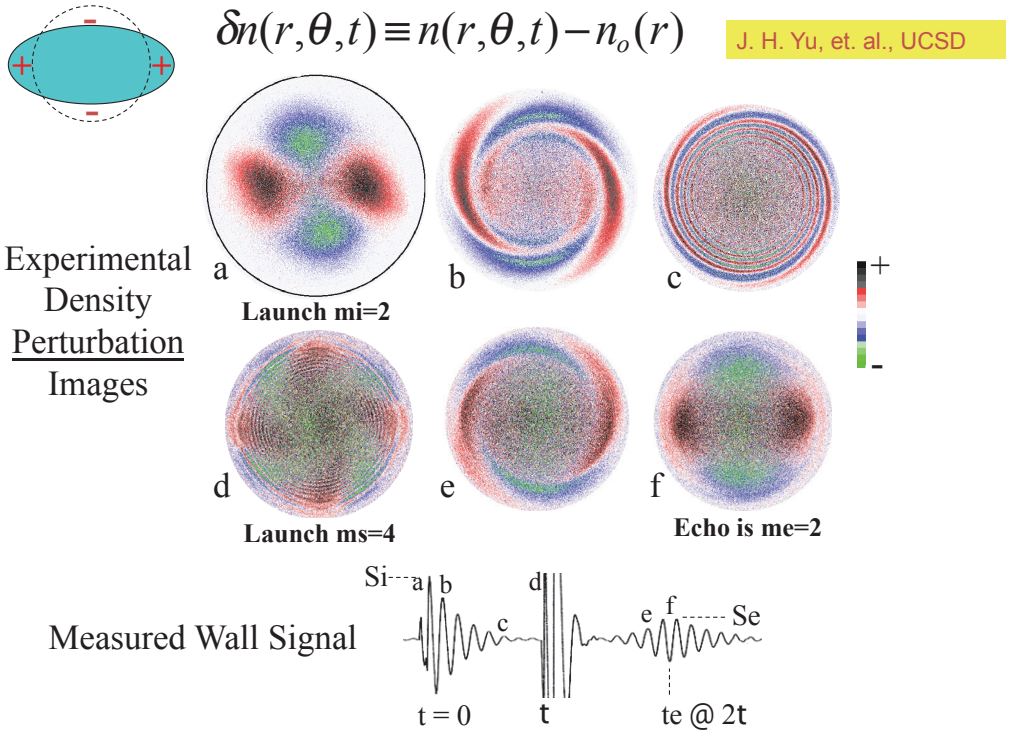

FIGURE 12. Experimental demonstration of the fluid echo.

ACKNOWLEDGEMENTS

As is apparent from the references, many people have contributed to the work that I have talked about today, and I want to give a special thanks to my long time collaborators at UCSD: Fred Driscoll, Dan Dubin, Cliff Surko, Francois Anderegg and Andrey Kabantsev. Also, special thanks goes to John Bollinger of the NIST ion storage group and to Roy Gould of Cal Tech with whom we have collaborated for many years. Over the years, research on nonneutral plasmas at UCSD has been supported by the NFS/DoE Partnership in Basic Plasma Science and Engineering and by the Office of Naval Research, where Chuck Roberson organized an ONR Research Initiative focused on the nonneutral plasmas.

REFERENCES

1. N. Rostoker and M. Rosenbluth, *Phys. Fluids* **3,** 1 (1960)
2. N. Rostoker, *Nucl. Fusion* **1**, 101 (1960)
3. N. Rostoker, *Phys. Fluids* **3,** 922 (1960)
4. M. Rosenbluth and N. Rostoker, *Phys. Fluids* **5,** 776 (1962)
5. T. O'Neil and N. Rostoker, *Phys. Fluids* **8,** 1109 1965)
6. T. M. O'Neil, *Phys. Fluids* **8**, 2255 (1965)

7. D. A. Schecter, D. H. E. Dubin, A. C. Cass, C. F. Driscoll, I. M. Lansky and T. M. O'Neil, *Phys. Fluids* **12,** 2397 (2000)
8. J. H. Yu, C. F. Driscoll and T. M. O'Neil, *Phys. Plasmas* **12,** 0055701: 1-8 (2005)
9. J. H. Malmberg, C. F. Driscoll, B. Beck, D. L. Eggleston, J. Fajans, K. S. Fine, X. P. Huang and A. W. Hyatt, *Non-neutral Plasma Physics* (C. W. Roberson and C. F, Driscoll, eds.) AIP Conf. Proc. **175** (1988)
10. T. M. O'Neil, *Physics Today* **52**, 24 (1999)
11. R. C. Davidson, *Physics of Nonneutral Plasmas* (Addison-Wesley, Redwood City, CA) (1990)
12. D. H. E. Dubin and T. M. O'Neil, *Rev. Mod. Phys.* **71**, 87 (1999)
13. Personal communication: F. Anderegg and C. F. Driscoll, UCSD
14. A. Kuley, Z. F. Wang, Z. Lin and F. Wessel, *Phys. Plasmas* **20**, 10(2013); A. Necas, *Electrostatic current drive for a field reversed configuration,* Phd. Thesis, University of California at Irvine, Department of Physics and Astronomy, (2007)
15. S. Ichimaru, *Rev. Mod. Phys.* **54**, 1017 (1982)
16. J. J. Bollinger, J. B. Mitchell, X. P. Huang, W. M. Itano, J. N. Tan, B. M. Jelenkovic and J. D. Wineland, *Phys. Plasmas* **7**, 7 (2000)
17. N. Rostoker, *Phys. Fluids* **7**, 479 (1964)
18. E. E. Salpeter, *Aust. J. Phys.* **7**, 373 (1954)
19. T. M. O'Neil and P. J. Hjorth, *Phys. Fluids* **28**, 3241 (1985); M. E. Glinsky, T. M. O'Neil, M. N. Rosenbluth, K. Tsuruta and I. Ichimaru, *Phys. Fluids B* **4**, 1156 (1992); B. R. Beck, J. Fajans and J. H. Malmberg, *Phys. Plasmas* **4**, 1250 (1996)
20. D. H. E. Dubin, *Phys. Rev. Lett.,* **94**, 025001 (2005)
21. F. Anderegg, D. H. E. Dubin, T. M. O'Neil and C. F. Driscoll, *Phys. Rev. Lett.* **102**, 185001 (2009); *Phys. Plasmas* **17**, 055702 (2010)
22. H. Dewitt and W. Slattery, *Contrib. Plasma Phys.* **39**, 97 (1999); A. Chugunov, H. E. Dewitt and D. G. Yakovlev, *Phys. Rev. D* **76**, 025028 (2007); S. Ogata, *Astrophys. J.* **481**, 883 (1997); S. Ogata, H. Iyetomi and S. Ichimaru, *ibid.* **372**, 259 (1991)
23. F. Anderegg, N. Shiga, D. H. E. Dubin, C. F. Driscoll and Roy Gould, *Phys. Plasmas* **10**, 1556 (2003)
24. C. F. Driscoll and K. S. Fine, *Phys. Fluids B* 2, 1359 (1990); T. B. Mitchell and C. F. Driscoll, *Phys. Fluids* **8**, 1828 (1996); A. A. Kabantsev and C. F. Driscoll, *IEEE Trans. On Plasma Science* **30**, 22 (2002); K. S. Fine, A. C. Cass, W. G. Flynn and C. F. Driscoll, *Phys. Rev. Lett.* **75**, 3277 (1995)
25. R. W. Gould, T. M. O'Neil and J.H. Malmberg, *Phys. Rev. Letters* **19**, 219 (1967); T. M. O'Neil and R. W. Gould, *Phys. Fluids* **11**, 134 (1968); J. H. Malmberg, C. B. Wharton, R.W. Gould and T. M. O'Neil, *Phys. Rev. Letters* **20**, 95 (1968)